Supplemental Material: Strong uniaxial pressure dependencies evidencing spin-lattice coupling and spin fluctuations in $Cr_2Ge_2Te_6$

S. Spachmann[1,a], S. Selter[2], B. Büchner[2,3], S. Aswartham[2,b], R. Klingeler[1,c]
[1] *Kirchhoff Institute for Physics, Heidelberg University, Heidelberg, Germany*
[2] *Leibniz Institute for Solid State and Materials Research (IFW), Dresden, Germany and*
[3] *Würzburg-Dresden Cluster of Excellence ct.qmat*
(Dated: April 21, 2023)

In the following

- a summary of anomalies in the magnetostriction and magnetization measurements for $B \parallel ab$ and resulting uniaxial pressure dependencies,
- the demagnetization factor and sample shape correction of magnetization measurements,
- the thermal expansion coefficient around T_C at low fields up to 0.2 T, as well as
- magnetostriction and magnetization data up to 15 T

are shown which support the results of our manuscript.

I. PRESSURE DEPENDENCE OF THE CRITICAL FIELD

A summary of the relevant anomalies obtained by dilatometry and magnetometry at the phase boundary of the low temperature and low field (LTF) phase ($B \parallel ab$) as well as the derived pressure dependencies of the critical field B_c are given in Table I.

Table I. Summary of anomalies in the magnetostriction and magnetization measurements for $B \parallel ab$ and derived uniaxial pressure dependence of the critical field.

T (K)	B_c (T)	$\Delta\lambda$ (10^{-5} T^{-1})	$\Delta(\partial M/\partial B)$ (μ_BT^{-1}Cr^{-1})	$\partial B_c/\partial p_{ab}$ (T/GPa)
2.25	0.46	19(3)	-4.6(5)	-1.25(18)
5.1	0.46	19(2)	-4.6(5)	-1.22(18)
10	0.46	19(2)	-4.5(5)	-1.26(18)
19.8	0.43	19(2)	-4.5(5)	-1.24(18)
29.7	0.406	18(2)	-4.7(6)	-1.19(17)
39.7	0.37	18(2)	-4.8(6)	-1.11(16)
49.6	0.315	19(2)	-5.2(7)	-1.07(16)
59.3	0.226	24(2)	-5.4(7)	-1.33(19)

[a] sven.spachmann@alumni.uni-heidelberg.de
[b] s.aswartham@ifw-dresden.de
[c] klingeler@kip.uni-heidelberg.de

II. CORRECTIONS FOR MAGNETIZATION MEASUREMENTS

Measurements of the isothermal magnetization were performed on a thin sample with dimensions of $2.0 \times 1.3 \times 0.235$ mm^3 and a mass of $m = 3.27(5)$ mg. The measured magnetization was corrected for the demagnetizing field using demagnetization factors of $N = 0.746$ for $B \parallel c$ and $N = 0.099$ for $B \parallel ab$ (Fig. S1(a) and (b)). Further correction factors due to the sample geometry were obtained based on the experimental data of a square nickel film [1]. To extract correction factors for the side lengths of 2.0 mm and 1.3 mm a square of equal area with a side length of 1.65 mm was assumed. For measurements with $B \parallel c$, i.e., along the thin direction, power-law fits to the data provided in Ref. [1] for vibration amplitudes of 1.0 mm to 5.0 mm yielded the correction factor f at 1.65 mm at different amplitudes. A linear interpolation of these data points resulted in $f = 1.086$ for the amplitude of 1.8 mm at which all measurements were performed. For a vertical alignment of the sample, with $l_{ab} = 1.3$ mm and $B \parallel ab$, third-order polynomial fits were applied to extract f at different vibration amplitudes. A linear interpolation of the resulting values for the different amplitudes yielded $f = 1.061$ for an amplitude of 1.8 mm. The effect of the corrections is shown in Fig. S1(d).

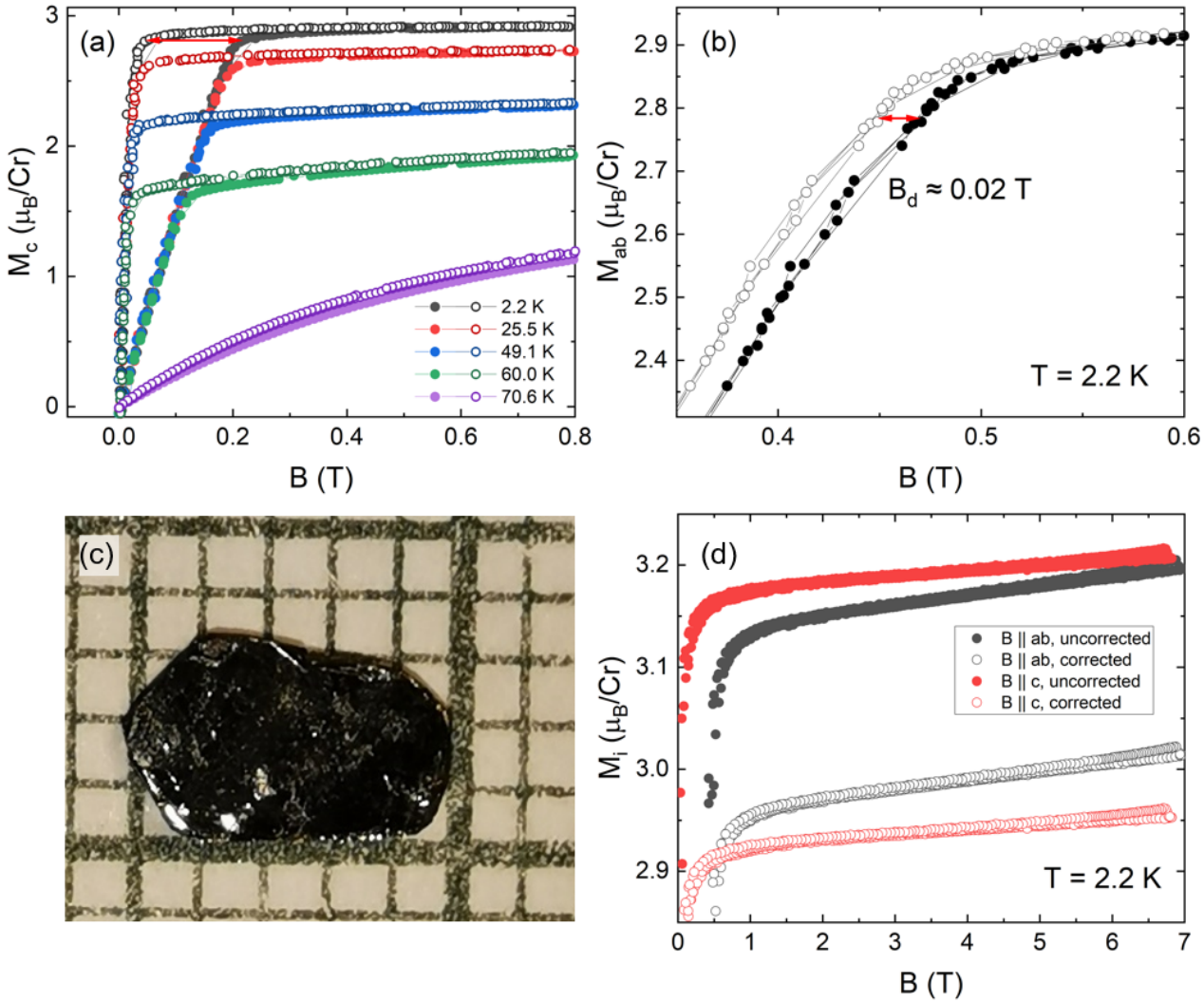

Figure S1. (a, b) Demagnetization factor correction with (a) $N = 0.746$ for $B \parallel c$ and (b) $N = 0.099$ for $B \parallel ab$. Red horizontal arrows give an impression of the demagnetization field. (c) $Cr_2Ge_2Te_6$ sample used for the c axis thermal expansion measurements. (d) Example for the effect of the magnetization correction due to sample geometry. Closed (open) symbols mark the uncorrected (corrected) data in (a), (b) and (d).

III. FURTHER MAGNETOSTRICTION AND MAGNETIZATION DATA

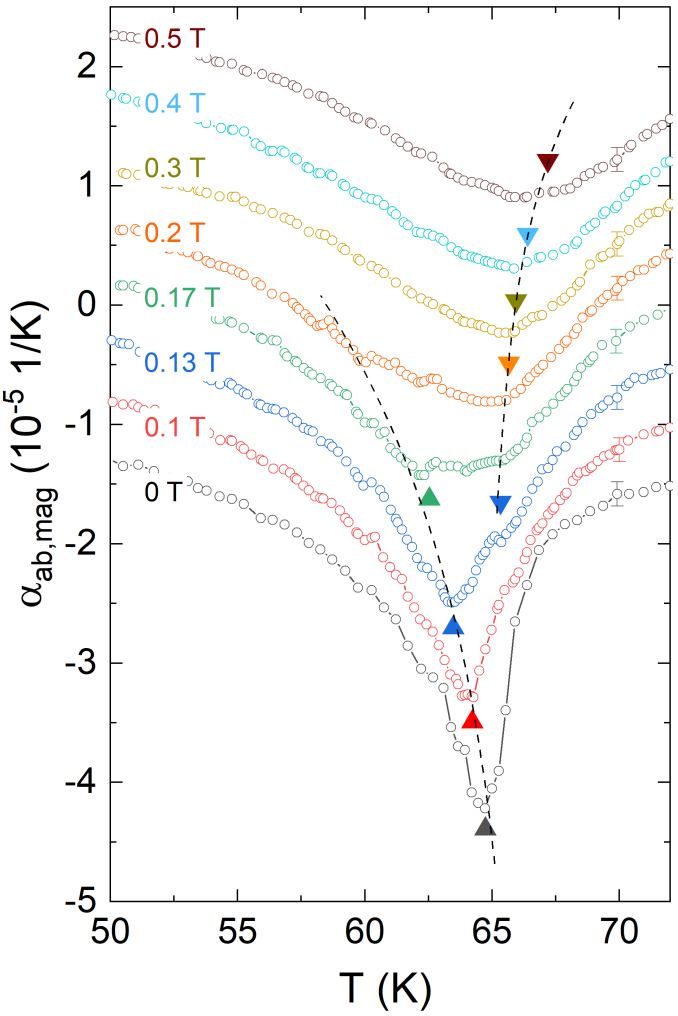

Figure S2. Magnetic contributions to the thermal expansion coefficient in external fields $B \parallel ab \leq 0.5$ T (i.e., further enlargement of Fig. 1d in the main manuscript). Curves are offset by 5×10^{-6}/K for clarity. Triangles nd dashed lines indicate trends of anomalies. The data show the initial suppression of the main peak, the development of a shoulder-anomaly at 0.13 T, and non-symmetric broadening of the upper peak as well as suppression of lower feature and shift of the upper anomaly to higher temperatures at $B \leq 0.2$ T.

A quadratic fit to the relative length changes $\Delta L_{ab}(B)$ in the LTF phase is shown in Fig. S3(a). Fig. S3 shows a comparison of the temperature dependence of the refined magnetic moment of Cr^{3+} ions [2] to the proportionality constant $a(T)$ for the quadratic-in-field magnetostriction at different temperatures below T_C. Fits up to fourth order of the relative length changes with respect to magnetization below B_c, $\Delta L_{ab}(M,T) = A_1(T)M^2 + A_2(T)M^4$, are shown in Fig. S3(c).

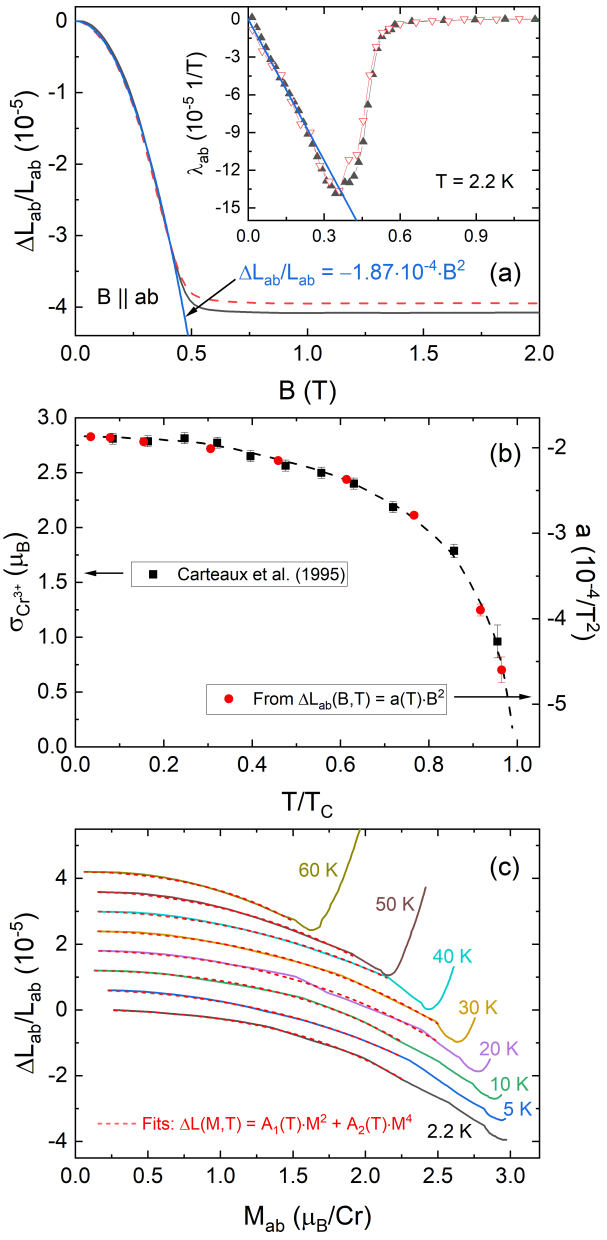

Figure S3. (a) Magnetostriction of the in-plane direction ($B \parallel ab$) at $T \approx 2\ K$. The inset shows the corresponding magnetostriction coefficient. The black line and triangles mark the up-sweep, the dashed red line and empty red triangles the down-sweep. The blue curve indicates a fit to a quadratic-in-field behavior. (b) Refined moment of Cr^{3+} ions (left axis, digitized from Ref. 2) vs. proportionality factor $a(T)$ for quadratic-in-field magnetostriction $\Delta L_{ab}/L_{ab}$. The dashed line is a guide to the eye taken also from Ref. 2. (c) In-plane relative length changes as a function of in-plane magnetization. Data are shifted vertically by $6 \cdot 10^{-6}$ for better visibility. Red dashed lines indicate fits $\Delta L = A_1(T) \cdot M_{ab}^2 + A_2(T) \cdot M_{ab}^4$.

Fig. S4 shows the magnetostriction and magnetostriction coefficients for $B \parallel c$ at various temperatures below T_C (a, b) as well as magnetization measurements at temperatures from 2 to 204 K (c, d).

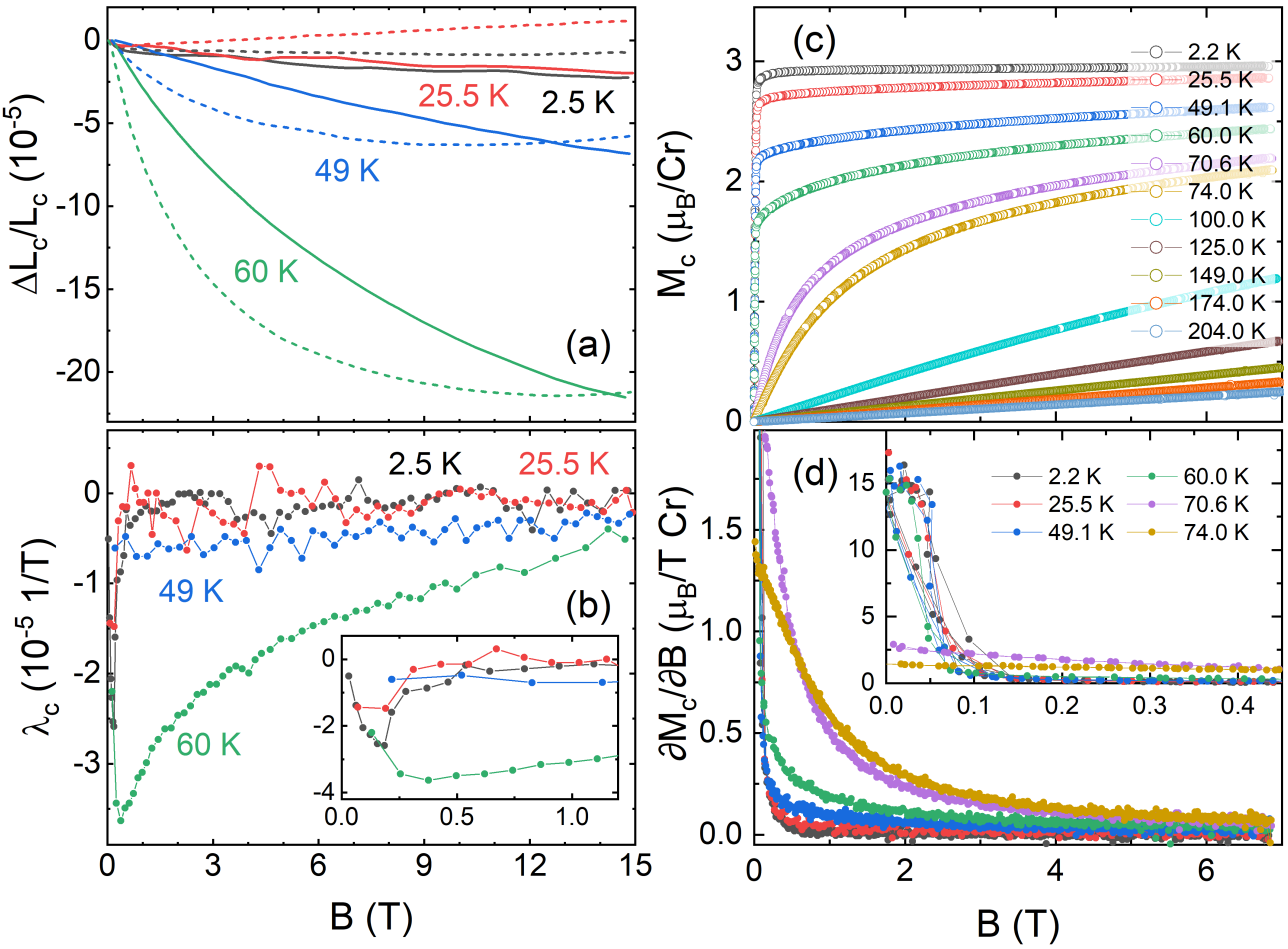

Figure S4. Comparison of magnetostriction (a, b) and magnetization (c, d) for $B \parallel c$. (a) Relative length changes and (b) magnetostriction coefficient for temperatures from 2 K to 60 K. (c) Isothermal magnetization and (d) magnetic susceptibility at different temperatures up to 204 K. Magnetization data was corrected for demagnetization effects whereas magnetostriction data is shown as measured.

Magnetostriction and magnetostriction coefficients for $B \parallel ab$ at various temperatures below T_C as well as magnetization measurements at temperatures from 2 to 199 K are shown in Fig. S5.

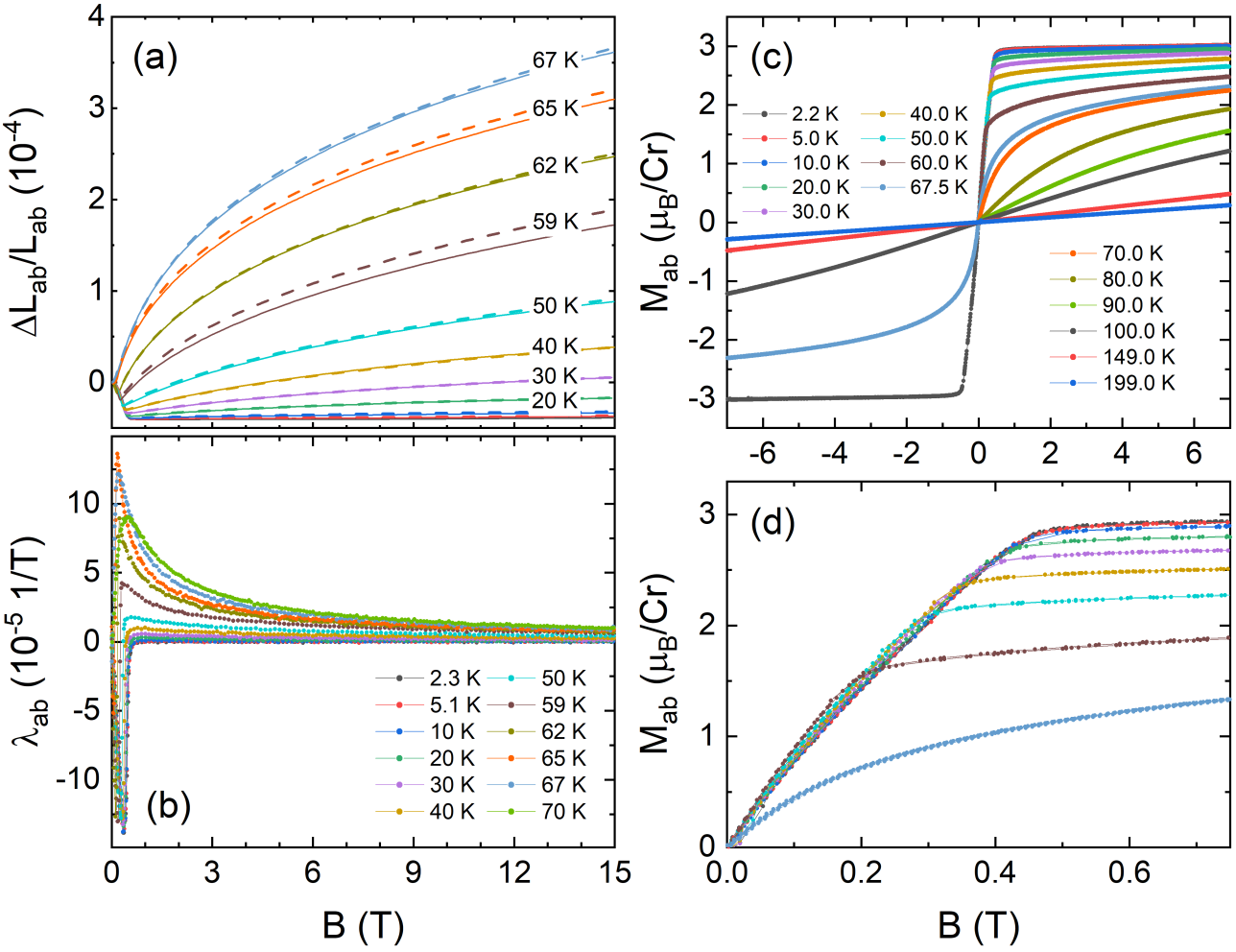

Figure S5. Comparison of magnetostriction (a, b) and magnetization (c, d) for $B \parallel ab$. (a) Relative length changes and (b) magnetostriction coefficient for temperatures from 2 K to 70 K. (c) Isothermal magnetization, and (d) magnetic susceptibility at different temperatures up to 199 K. Magnetization data was corrected for demagnetization effects whereas magnetostriction data is shown as measured.

Magnetostriction measurements of $B \parallel ab, c$ above T_C are shown in Fig. S6. Both up- and down-sweeps are shown. Up-sweeps are taken from Ref. [3]. While hysteresis is negligible for $B \parallel ab$, significant hysteresis is visible for $B \parallel c$ between 70 and 200 K.

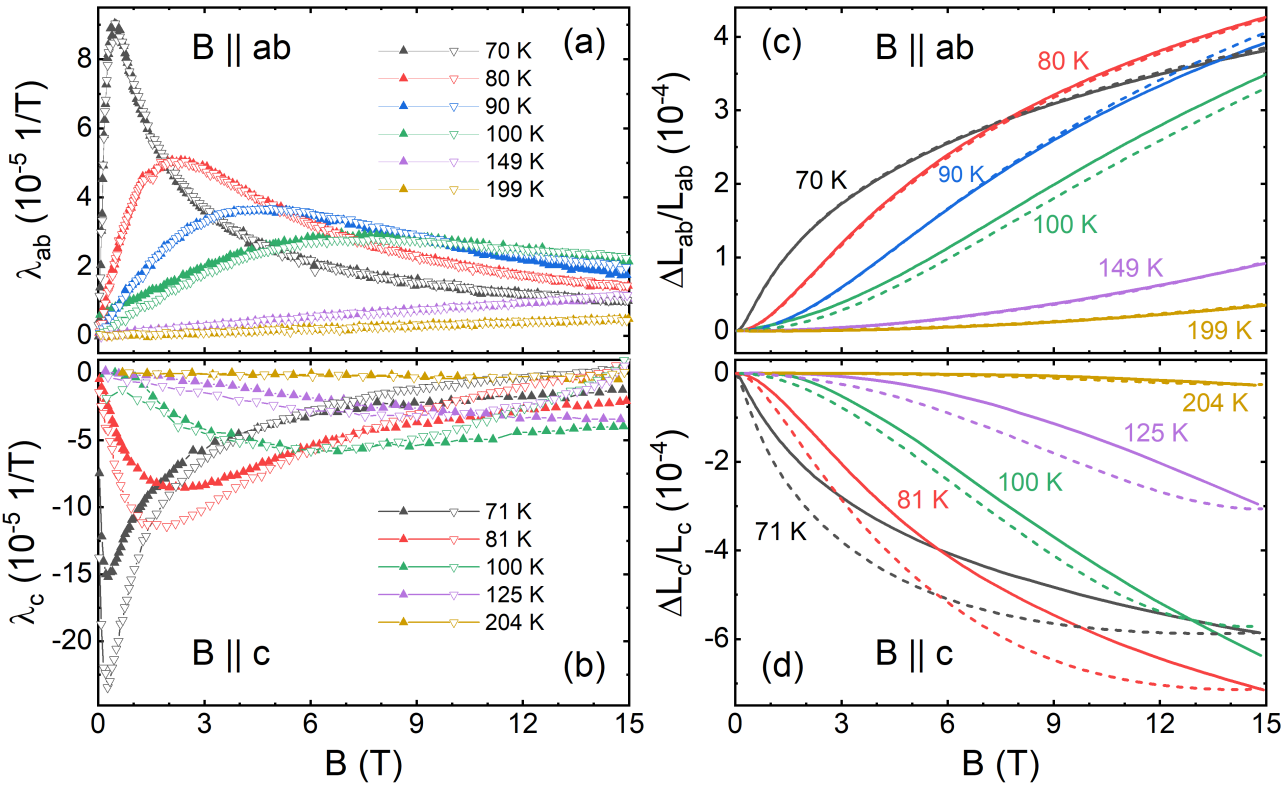

Figure S6. (a, b) Magnetostriction coefficients and (c, d) magnetostrictive relative length changes for $B \parallel ab$ (a, c) and $B \parallel c$ (b, d) at temperatures $T > T_C$. Filled upward triangles and solid lines mark up-sweeps, empty downward-triangles and dashed lines mark down-sweeps. Up-sweeps are taken from Ref. [3].

[1] Quantum Design, Accuracy of the reported moment: Sample shape effects, SQUID-VSM Application Note 1500-015 ((Quantum Design, 2010)).

[2] V. Carteaux, D. Brunet, G. Ouvrard, and G. Andre, Crystallographic, magnetic and electronic structures of a new layered ferromagnetic compound $Cr_2Ge_2Te_6$, Journal of Physics: Condensed Matter **7**, 69 (1995).

[3] S. Spachmann, A. Elghandour, S. Selter, B. Büchner, S. Aswartham, and R. Klingeler, Strong effects of uniaxial pressure and short-range correlations in $Cr_2Ge_2Te_6$, Physical Review Research **4**, L022040 (2022).